Published in final edited form as:
Cell. 2008 September 5; 134(5): 769–781. doi:10.1016/j.cell.2008.06.037.

Proteostasis Regulators and Pharmacologic Chaperones Synergize to Correct Protein Misfolding Diseases

Ting-Wei Mu[1,4], **Derrick Sek Tong Ong**[1,4], **Ya-Juan Wang**[1,2], **William E. Balch**[3], **John R. Yates**[2], **Laura Segatori**[1,4,5,*], and **Jeffery W. Kelly**[1,*]

1*Department of Chemistry and The Skaggs Institute for Chemical Biology, The Scripps Research Institute, La Jolla, CA 92037*

2*Department of Chemical Physiology, The Scripps Research Institute, La Jolla, CA 92037*

3*Department of Cell Biology, The Scripps Research Institute, La Jolla, CA 92037*

Summary

Loss-of-function diseases are often caused by a mutation in a protein traversing the secretory pathway that compromises the normal balance between protein folding, trafficking and degradation. We demonstrate that the innate cellular protein homeostasis, or proteostasis, capacity can be enhanced to fold mutated enzymes that would otherwise misfold and be degraded, using small molecule proteostasis regulators. Two proteostasis regulators are reported that alter the composition of the proteostasis network in the endoplasmic reticulum through the unfolded protein response, increasing the mutant folded protein concentration that can engage the trafficking machinery, restoring function to two non-homologous mutant enzymes associated with distinct lysosomal storage diseases. Co-application of a pharmacologic chaperone and a proteostasis regulator exhibits synergy because of the former's ability to further increase the concentration of trafficking competent mutant folded enzymes. It may be possible to ameliorate loss-of-function diseases by using proteostasis regulators alone or in combination with a pharmacologic chaperone.

Introduction

Cellular protein homeostasis, or proteostasis, involves controlling the conformation, concentration, binding interactions, and location(s) of individual proteins making up the proteome, by way of conserved pathways making up the proteostasis network. Since proteins enable physiology, loss of cellular proteostasis influences or causes numerous diseases that should be correctable by restoring proteostasis (Albanese et al., 2006; Brown et al., 1997; Cohen and Kelly, 2003; Deuerling and Bukau, 2004; Horwich et al., 2004; Imai et al., 2003; Kaufman, 2002; Ron and Walter, 2007; Young et al., 2004; Balch et al., 2008). Loss-of-function diseases often result from the inability of a mutated protein to fold efficiently within the secretory pathway, leading to extensive endoplasmic reticulum (ER) associated degradation (ERAD) and to a lowered concentration of the protein at its destination (Brodsky, 2007; Brown et al., 1997; Cohen and Kelly, 2003; Moyer and Balch, 2001; Schroeder and Kaufman, 2005; Ulloa-Aguirre et al., 2004; Wang et al., 2006; Wiseman et al., 2007).

*To whom correspondence should be addressed. Telephone: 858-784-9605, Fax: 858-784-9610, E-mail: jkelly@scripps.edu, segatori@rice.edu.
[4]These authors contributed equally to this work.
[5]Current Address: Department of Chemical and Biomolecular Engineering, Rice University, 6100 Main Street, MS-362, Houston, TX 77005

Loss-of-function lysosomal storage diseases (LSDs) are often caused by extensive ERAD of a mutated lysosomal enzyme instead of proper folding and trafficking (Fan, 2001; Fan et al., 1999; Futerman and van Meer, 2004; Sawkar et al., 2002; Sawkar et al., 2006a; Schmitz et al., 2005). LSDs are characterized by enzyme substrate accumulation, typically arising when the activity of the mutated enzyme drops below ≈ 10% of normal (Conzelmann and Sandhoff, 1984; Schueler et al., 2004).

LSDs are now treated by enzyme replacement (Beutler et al., 1977; Brady, 2006), not applicable to neuropathic LSDs because recombinant enzymes do not cross the blood brain barrier. Many mutated lysosomal enzymes associated with LSDs can fold and exhibit partial activity under appropriate conditions, such as when the cells are grown at a lower permissive temperature (Futerman and van Meer, 2004). The challenge for most LSD-associated enzymes is to fold in the neutral pH environment of the ER, distinct from that of the acidic environment of the lysosome (Sawkar et al., 2006b).

We wondered whether it would be possible to restore partial folding, trafficking and function to misfolding and ERAD-prone mutated lysosomal enzymes by adapting the innate cellular biology of proteostasis, using small molecules or biologicals that enhance cellular proteostasis, so-called “proteostasis regulators” (PRs) (Balch et al., 2008). These function by manipulating signaling pathways, including the unfolded protein response (UPR), resulting in transcriptional and translational upregulation of proteostasis network components in the ER (e.g. macromolecular chaperones) or through a Ca^{2+} signaling proteostasis pathway (Mu et al., 2008).

The proteostasis network supports the folding and trafficking of numerous lysosomal enzymes, thus a single PR should be able to restore proteostasis in multiple LSDs and possibly related loss-of-function diseases (Balch et al., 2008). PRs should enhance the established utility of pharmacologic chaperones (PCs) that bind the folded mutant proteins in the ER (Bouvier, 2007; Fan et al., 1999; Sawkar et al., 2002) because they would increase the concentration of the folded mutant protein in the ER for PCs to bind.

We focus on identifying PRs that function in patient-derived fibroblasts from dissimilar LSDs. The most common LSD, Gaucher disease, is often caused by N370S or L444P glucocerebrosidase (GC) mutations that lead to extensive ERAD and loss of GC function in the lysosome, resulting in glucosylceramide accumulation (Beutler et al., 2005; Sawkar et al., 2006a). The L444P GC mutation that often leads to neuropathic Gaucher disease does not respond significantly to PCs (unlike the N370S variant), because of the very low concentration of folded L444P GC in the ER (Sawkar et al., 2005; Yu et al., 2007). Tay-Sachs disease, another LSD, is caused by β-hexosaminidase A (HexA) mutations (Jeyakumar et al., 2002). The α-subunit G269S mutation compromises its folding, leading to substantial α-subunit ERAD, reducing its availability to form the HexA heterodimer (Maegawa et al., 2007), leading to neuronal storage of GM2 gangliosides, the HexA substrate. The folding, trafficking and activity of HexA is known to be partially restored in patient-derived fibroblasts harboring the α-subunit G269S mutation upon active site-directed PC treatment (Maegawa et al., 2007; Tropak et al., 2004).

Herein, we report two PRs that each partially restore mutant GC and HexA folding, trafficking and function in Gaucher and Tay-Sachs patient-derived cell lines-providing proof of principle that it is possible to treat two LSDs with a single PR. While these PRs activate both the heat shock response (HSR) (influencing cytoplasmic proteostasis) and the UPR (affecting secretory pathway proteostasis), activation of the UPR appears to be necessary and sufficient for PR function. Moreover, in two different LSDs we demonstrate that co-application of a PR and a PC yields a synergistic restoration of mutant enzyme function in patient-derived fibroblasts,

owing to a PR-mediated increase in folded mutant enzyme concentration in the ER, providing more folded mutant enzyme for the PC to bind to, which further increases the lysosomal enzyme concentration.

Results

Celastrol is a PR in Gaucher disease patient-derived fibroblasts

We administered molecules known to influence proteostasis, including salubrinal (Boyce et al., 2005), celastrol (Westerheide et al., 2004), indomethacin, and sodium salicylate, to L444P GC Gaucher fibroblasts. Lysosomal GC activity was evaluated using the intact fibroblast assay, employing the synthetic substrate 4-methylumbelliferyl β-D-glucoside (Sawkar et al., 2002). Activities are reported as a fold-change relative to mutant GC activity in untreated cells and as the fraction of WT GC activity (See Figure 1C inset for lysosomal GC variant activities, a consequence of lowered specific activity and a lowered lysosomal concentration) (Sawkar et al., 2005).

Celastrol (0.8 μM), but not the other compounds evaluated, increased the activity of L444P GC 1.8-fold (to 23% of the cellular WT GC activity (referred to as “WT activity” hereafter)) after 72 h at 37°C (Figure 1A); notable because we had never observed a statistically significant increase in L444P GC activity using PCs (Sawkar et al., 2005). Celastrol is known to be a heat shock transcription factor 1 (HSF1) activator—inducing the HSR in human cells (Westerheide et al., 2004), upregulating cytoplasmic proteostasis network components (Lindquist, 1986; Westerheide and Morimoto, 2005).

Partial restoration of L444P GC proteostasis was further supported by Western blot analysis of the glycosylation pattern of GC after treatment with endoglycosidase H (endo H) (Figure 1B) (Ron and Horowitz, 2005). Digestion with Peptide N-Glycosidase F (PNGase F), an amidase that cleaves the innermost GlcNAc from the Asn side chain, confirms that the high molecular weight (MW) endo H resistant band was glycosylated (Figure S1). A low MW band corresponding to the endo H-sensitive, partially glycosylated GC that has not left the ER is typically detected after endo H treatment (Ron and Horowitz, 2005; Sawkar et al., 2006b; Schmitz et al., 2005). A high MW band corresponding to the endo H-resistant lysosomal GC glycoform is observed for WT fibroblasts (Figure S1, lane 2), but only faintly, if at all, for untreated Gaucher disease-associated GC variants (Figure 1B) (Ron and Horowitz, 2005; Sawkar et al., 2006b; Schmitz et al., 2005). Increased L444P GC in celastrol treated fibroblasts is a mixture of enzymatically active, natively folded, and natively glycosylated GC (black bars, Figure 1B), and ER retained GC that is not properly glycosylated (white bars, Figure 1B).

Celastrol treatment (< 0.8 μM, 72 h) of Gaucher fibroblasts harboring N370S or G202R GC mutations (known to be retained in the ER) revealed a 1.5-fold increase in GC enzymatic activity (to ≈ 39% of WT activity) and a 1.9-fold increase (to ≈ 20% of WT activity), respectively (Figure 1C). It is notable that the activity of L444P GC, a severe neuropathic mutation, is restored by celastrol to the same extent as the activity of N370S GC. L444P GC fibroblasts exposed to celastrol every 24 h for 96 h exhibited a 2.1-fold increase in activity (to ≈ 26% of WT activity) at 120 h (0.2 μM Celastrol) (Figure S2A). Celastrol increased L444P GC activity for 96 h after a single dose and for 120 h with multiple doses (Figures S2B and S2C). To probe whether celastrol influenced other lysosomal enzymes, the cellular activity of 7 WT lysosomal enzymes were compared in untreated and celastrol treated L444P fibroblasts. Celastrol treatment did not increase the enzymatic activity of these sentinel enzymes by more than 10% (Figure S3, right panel), and in a separate WT fibroblast experiment, WT GC levels were unaltered by celastrol.

Immunofluorescence microscopy reveals that WT GC colocalized with the lysosomal marker LAMP2 (Figure 1D, top row, GC in green, LAMP2 in red, overlap artificially colored white) verifying the trafficking of WT GC to the lysosome (Sawkar et al., 2006b). L444P GC fibroblasts were incubated without and with 0.8 μM celastrol for 3 d prior to plating for microscopy. L444P GC was barely visible without drug treatment (extensive ERAD), but was easily detected after celastrol treatment (Figure 1D, cf. row 3 with row 2) and exhibited colocalization with the lysosomal marker. In summary, celastrol partially corrects the folding, trafficking and activity deficits of L444P GC.

MG-132 is a PR in Gaucher disease patient-derived fibroblasts

Because proteasome inhibitors both enhance chaperone expression levels (Bush et al., 1997; Liao et al., 2006) and inhibit ERAD (Chillaron and Haas, 2000), they could function as PRs (Wiseman et al., 2007). To test this hypothesis, L444P GC fibroblasts were subjected to a single exposure of the known proteasome inhibitors MG-132, lactacystin, PS I, PS IV, and Tyropeptin A. PS IV, lactacystin, and Tyropeptin A did not enhance L444P GC activity (Figure S4). PS I resulted in a modest 1.25-fold increase (Figure S4A). In contrast, MG-132 increased L444P GC activity 4-fold (to ≈ 50.0% of WT activity) after 120 h (Figure 1E). Western blot analysis revealed a striking increase in the endo H-resistant L444P GC band upon MG-132 treatment, especially after 72 h (Figure 1F, black bars). Immunofluorescence microscopy of MG-132 (0.25 μM, 72 h) treated L444P GC fibroblasts revealed enhanced lysosomal colocalization (Figure 1D, cf. row 4 with 2). To probe whether MG-132 influenced other lysosomal enzymes, the cellular activity of 7 WT lysosomal enzymes were compared in untreated and MG-132 treated cells. MG-132 increased the activity of α-galactosidase 1.8-fold, whereas the activity of other sentinel enzymes monitored increased an average of 1.2-fold (Figure S3, left panel). In summary, MG-132 also partially corrects the folding, trafficking and activity deficits of L444P GC.

Mass spectrometry-based proteomic analysis (Multidimensional Protein Identification Technology, (MudPIT)) was used to understand the influence of PR treatment on global protein biogenesis (Liu et al., 2004; Liao et al., 2007; Rikova et al., 2007; see supplemental experimental procedure). Treatment of L444P GC fibroblasts with MG-132 (0.8 μM) for 3 d upregulated 198 proteins and down regulated 255 proteins, while treatment with celastrol (0.8 μM) for 3 d upregulated 199 proteins and down regulated 292 proteins, amongst the 2100 proteins detected in the untreated and treated samples (Figure 2A). This demonstrates that PR treatment can provide a corrective environment for energetically destabilized enzymes with modest effects on the proteome.

Proteasome inhibition does not appear to be sufficient for GC PR function

Since MG-132 is an established proteasome inhibitor and because celastrol has recently been reported to inhibit the proteasome, this is a possible basis for their PR function (Yang et al., 2006). L444P GC fibroblasts were incubated with MG-132, lactacystin or celastrol as a function of concentration for 2 h before measurement of the chymotrypsin-like activity of the proteasome–experiments that yielded half maximal inhibitory concentrations (IC_{50}s) of 44.1 ± 5.4 nM, 58.1 ± 6.4 nM, and 17.2 ± 2.1 μM, respectively (Figure 2B). MG-132 (0.25 μM) treatment of L444P GC fibroblasts led to 93 and 92% chymotrypsin-like activity inhibition after 1 and 3 d, while celastrol (0.8 μM) treatment afforded 52 and 27% inhibition after 1 and 3 d, respectively (Figure 2C). Administration of MG-132 (0.8 μM) or celastrol (0.8 μM) to L444P GC fibroblasts for 1 and 3 d led to the accumulation of ubiquitinated proteins (Figure 2D), more so in the case of MG-132 treatment, indicating that protein turnover was inhibited. While it is clear that MG-132 strongly inhibits the chymotrypsin-like activity of the proteasome at the concentrations employed for PR function, the nearly exact dose response curve of the more selective proteasome inhibitor lactacystin (Figure 2B), a compound that is not a GC PR

(Figure S4B), suggests that inhibiting the chymotrypsin-like activity of the proteasome is not sufficient for GC PR function. That another activity possessed by celastrol and MG-132 explains their PR function is also supported by our observation that other potent proteasome inhibitors (PS IV and Tyropeptin A) did not enhance L444P GC proteostasis at all. While proteasome inhibition does not appear to be a major contributor to PR function, it could augment the UPR activator function of PRs discussed below.

MG-132 and celastrol activate the HSR and the UPR based on chaperone level increases

It is known that celastrol and MG-132 induce the heat-shock response (HSR), enhancing the proteostasis capacity of the cytosol (Bush et al., 1997; Liao et al., 2006; Morimoto, 1998; Westerheide et al., 2004) and it is possible that they induce one or more of the three arms of the unfolded protein response (UPR) that remodels the proteostasis network within the ER (and possibly the secretory pathway) to be more pro-folding and export permissive (Ron and Walter, 2007; Schroeder and Kaufman, 2005). To monitor the extent to which the HSR and the UPR were induced by PR treatment, quantitative reverse transcription-polymerase chain reaction (RT-PCR) analysis of chaperone transcription was performed using the primers listed in Table S1. L444P GC cells were incubated without and with 0.8 μM MG-132 or 0.8 μM celastrol for 24 h, prior to total RNA extraction, a time point at which substantial enhancement of GC activity was observed (Figures 1A and E). The relative mRNA levels of representative cytoplasmic HSR-associated chaperones (Hsp40, Hsp70, Hsp90, Hsp27, αB-crystallin), ER lumenal UPR-associated chaperones (BiP, GRP94, calreticulin), and the ER chaperone calnexin are shown in Figures 3A and B. Glyceraldehyde-3-phosphate dehydrogenase (GAPDH) levels, monitored as a housekeeping control, were unchanged in treated and untreated cells.

Treatment with either PR upregulates both cytoplasmic and ER lumenal chaperones. Both PRs significantly upregulated the mRNA expression levels of Hsp40, Hsp70, Hsp90, and αB-crystallin in the cytosol as well as BiP in the ER lumen although neither altered transcription of GRP94 (usually upregulated by the UPR) and calreticulin (Figures 3A and B). Differences also exist, as celastrol increased transcription of Hsp27 significantly, whereas MG-132 treatment did not. Conversely, MG-132 treatment upregulated the transcription of calnexin significantly, but celastrol treatment did not. These changes were confirmed at the protein level using Western blot analysis (Figures 3C and D), with the exception that calnexin protein levels remain unchanged upon MG-132 treatment, despite the 2 fold increase in its mRNA levels.

Since HSF1 may be responsible for celastrol's induction of the HSR (Westerheide et al., 2004), we monitored HSF1 levels by Western blot analysis in L444P GC fibroblasts after treatment with celastrol or MG-132 for the indicated period (Figure 3E). As reported, celastrol increased HSF1 levels over the 24 h period, while HSF1 levels even decreased slightly with MG-132 treatment over the same time course, consistent with reports that MG-132 induces the HSR without significantly upregulating HSF1 (Awasthi and Wagner, 2005; Bush et al., 1997).

Celastrol and MG-132 activate the three arms of the UPR

The ER responds to the accumulation of unfolded proteins by activating up to three integrated intracellular signaling pathways, collectively referred to as the UPR—regulating the expression of numerous genes that function within the secretory pathway (Ron and Walter, 2007; Schroeder and Kaufman, 2005). To explore whether the UPR was activated upon celastrol or MG-132 treatment, we monitored three well-established UPR-associated stress sensors: IRE1, ATF6, and PERK, integral membrane proteins that sense folding stress in the ER and transmit a signal across the ER membrane to the cytoplasm and into the nucleus, ultimately resulting in transcriptional activation (Ron and Walter, 2007; Schroeder and Kaufman, 2005).

IRE1 responds to stress by oligomerization, resulting in trans-autophosphorylation that activates its endonuclease function, precisely splicing the mRNA that encodes the transcription factor XBP1 (Ron and Walter, 2007; Schroeder and Kaufman, 2005). The spliced form of Xbp-1 was detected by RT-PCR in L444P GC fibroblasts after a 24 h incubation with MG-132 (0.8 μM) and after a 6 or 24 h incubation with celastrol (0.8 μM), indicating activation of the IRE1 arm of the UPR (Figure 4A). As a positive control, L444P GC fibroblasts were treated with tunicamycin (10 μg/ml) (Tm, Figure 4A, lane 1).

ATF6 responds to stress by regulated proteolysis in the Golgi, liberating a cytosolic fragment of ATF6 that activates a subset of UPR genes (Ron and Walter, 2007; Schroeder and Kaufman, 2005). Cleavage of ATF6 was monitored by Western blot analysis (Figure 4B). As positive controls, application of thapsigargin (Tg,1 μM, lane 2) and Tm (10 μg/ml, lane 3) increased the expression level of the cleaved and activated 50 kD form of ATF6, as well as increasing the expression level of the full length 90 kD form. The 50 kD form of ATF6 was significantly upregulated after the application of either PR (0.8 μM) from 2 to 24 h in L444P GC fibroblasts, indicating that MG-132 and celastrol both activated the ATF6 arm of the UPR.

PERK responds to stress by oligomerization and phosphorylation of the α subunit of eIF2, which leads to ATF4-mediated production of CHOP and other proteins, including chaperones (Ron and Walter, 2007; Schroeder and Kaufman, 2005). PR (0.8 μM) treatment upregulated the mRNA level of CHOP significantly, as discerned by quantitative RT-PCR analysis (Figure 4C), indicating PERK activation. In summary, both celastrol and MG-132 activate all three arms of the UPR (IRE1, ATF6, and PERK).

The UPR appears to be necessary and sufficient for MG-132 and celastrol L444P GC PR function

Since the UPR and HSR are activated by both PRs, we used siRNA treatment to discern the stress-associated signaling pathway(s) that are functionally important for L444P GC PR activity. siRNAs against HSF1 (responsible for the HSR) or IRE1α or ATF6 or PERK (the three arms of the UPR) were co-administered one at a time along with a PR. The experiment involves a 24 h siRNA pretreatment of L444P GC fibroblasts followed by 24 h of PR treatment in DMSO (along with DMSO vehicle controls). Western blot analysis revealed that HSF1, IRE1α, and ATF6 were silenced for 48 h after the transfection with the corresponding siRNA (Figure 5A, lane 3 for each) compared to the mock transfection (lane 1) or the negative control utilizing non-targeting siRNA (lane 2). Knockdown of IRE1α was further supported by the dramatically decreased Xbp-1 splicing induced by celastrol (Figure S5, cf. lanes 8, 9, 11). Gene knockdown of HSF1, ATF6, and PERK for at least 48 h after transfection was also verified by quantitative RT-PCR analysis (Figure 5B).

L444P GC fibroblasts were treated with the corresponding siRNA for 24 h and then MG-132 (0.25 μM in DMSO) for another 24 h before the intact cell GC activity assay or lysis for Western blot analysis was performed. L444P GC activity was increased when MG-132 was co-applied with non-targeting control siRNA (Figure 5C). Co-application of either HSF1 siRNA or ATF6 siRNA did not significantly diminish the GC activity increase afforded by MG-132 treatment (Figure 5C), indicating that HSF1 and ATF6 are not required for MG-132 PR function. Co-application of either IRE1α siRNA or PERK siRNA with MG-132 significantly diminished the GC activity increase (Figure 5C), indicating that the IRE1α and PERK UPR arms are important for MG-132 PR function.

GC Western blot analysis confirmed these observations. MG-132 increased the GC band intensity significantly when non-targeting control siRNA was co-applied (Figure 5D, cf. lanes 1 and 2). Co-application of MG-132 and either HSF1 siRNA or ATF6 siRNA did not significantly diminish the GC band intensity increase (Figure 5D, cf. lanes 3 and 4, and lanes

5 and 6). In contrast, co-application of either IRE1α siRNA and MG-132 or PERK siRNA and MG-132 significantly diminished the L444P GC band intensity increase (Figure 5D, cf. lanes 7 and 8, and lanes 9 and 10), consistent with the conclusion drawn above that IRE1α and PERK are required for MG-132 L444P GC PR function.

Western blot analysis of L444P GC levels demonstrated that co-application of celastrol and siRNAs directed against ATF6, IRE1α and PERK, but not HSF1 or non-targeting control siRNA, partially blocked celastrol's L444P GC PR function (Figure 5E). As for MG-132, the UPR appears to be critical for mediating the PR function of celastrol, but in this case all 3 arms of the UPR appear to be important.

PC and PR co-application exhibits synergistic rescue of mutant enzyme function

GC PCs stabilize the folded state ensemble in the ER, enabling a higher population of GC to engage the trafficking machinery and proceed to the lysosome (Sawkar et al., 2006b). Sub-inhibitory concentrations of GC inhibitors, such as N-(n-nonyl)deoxynojirimycin (NN-DNJ; <30 μM), serve as PCs to N370S and G202R GC Gaucher patient-derived fibroblasts increasing mutant GC folding and trafficking efficiency, as well as mutant GC activity (Sawkar et al., 2002; Sawkar et al., 2006b). Administration of NN-DNJ (5 μM) to N370S and L444P GC fibroblasts for 24 h or 120 h does not activate the UPR or the HSR in Gaucher fibroblasts, Figures S6 A–C, consistent with previous reports in Fabry fibroblasts (Yam et al., 2006), distinct from the PR function of celastrol and MG-132 (Figure 3–Figure 5). Therefore, co-application of a PC and a PR could have a synergistic effect on enhancing GC proteostasis, owing to the hypothesis that PR induction of the UPR creates a larger pool of folded mutant GC in the ER (Figures 1B and F) that the PC can bind and stabilize, further increasing the population of folded mutant GC•PC, which can engage the trafficking machinery along with the increased GC pool resulting from PR treatment (Bouvier, 2007; Fan et al., 1999; Sawkar et al., 2002).

A PC (NN-DNJ) and a PR (celastrol) were co-administered to fibroblasts harboring GC mutations known to be amenable to pharmacologic chaperoning (N370S and G202R GC), as a function of the concentration of each. G202R GC fibroblasts incubated with celastrol alone (0.4 μM) exhibited a 2-fold increase or a 100 unit or 100% increase in GC activity, while a 1.8-fold or 80 unit increase in G202R GC activity was observed with NN-DNJ (5 μM) alone (Figures S7A and B). Co-administration of celastrol (0.4 μM) and NN-DNJ (5 μM) resulted in a 4.2-fold or 320 unit increase in G202R GC activity (to ≈ 44% of WT activity) (Figure 6A), nearly double the 2.8-fold or 180 unit sum, demonstrating a synergistic enhancement of GC activity. An analogous synergistic increase (3.5 fold, ≈ 112% of WT activity) was observed when NN-DNJ (2.2 fold increase alone, Figure S7C) and celastrol (1.5 fold increase alone, Figure S7D) were co-applied to N370S GC fibroblasts (Figure 6B).

L444P GC is not amenable to PC rescue in fibroblasts under conditions where N370S and G202R GC respond, owing to its very low ER concentration and apparent susceptibility to inhibition (Sawkar et al., 2005). Pretreatment with celastrol, followed by a pulse of NN-DNJ and celastrol, followed by another celastrol treatment, capped by a pulse of NN-DNJ and celastrol was envisioned to enhance PR-directed UPR-mediated L444P GC folding in the ER, generating a higher steady state concentration of folded L444P GC for the PC to act on. Such a dosing schedule (Figure 6C) resulted in a 3.9-fold (290 unit) increase in L444P GC activity at 144 h (to 49% of WT activity), which is nearly 300% greater than the 2.0-fold or 100 unit sum, demonstrating a synergistic increase (also see Figures S8A and B).

To probe the generality of PC and PR synergy, NN-DNJ and MG-132 were co-administered to L444P GC fibroblasts using the optimized dosing protocol established for the synergistic use of celastrol and NN-DNJ. A synergistic 6.2-fold increase in L444P GC activity (to ≈ 78%

of cellular WT GC activity) was observed (MG-132 (0.4 μM) and NN-DNJ (0.5 μM)) (Figures 6D, and S9A and B).

Celastrol and MG-132 serve as PRs in Tay-Sachs cells-demonstrating LSD generality

Since celastrol and MG-132 appear to restore GC proteostasis through UPR-mediated upregulation of ER folding capacity, they should be able to enhance the folding, trafficking and function of other mutant enzymes associated with different lysosomal storage diseases. Mutations in the β-hexosaminidase A α-subunit can compromise ER folding resulting in extensive ERAD, leading to Tay-Sachs disease (Maegawa et al. 2007). The influence of PRs on HexA activity was studied in a compound heterozygous Tay-Sachs fibroblast cell line, harboring one of the most prevalent β-hexosaminidase A α-subunit mutations (G269S) and a second *HexA* allele (1278insTATC) incorporating a stop codon mutation into the coding region. Untreated αG269S HexA fibroblasts have 10% of the cellular WT HexA α-site activity, assessed using the MUGS substrate (Tropak et al., 2004). MG-132 administration (0.8 to 1 μM) led to a αG269S Hex α-site activity increase of 1.8-fold (to ≈ 18% of WT HexA Activity) 144 h after treatment (Figure 6E), while celastrol (0.4 to 0.6 μM) afforded a 1.6-fold increase (to ≈ 16% of WT HexA activity) after 96 h (Figure S10A). Treatment of a lung cell line expressing the ΔF508 CFTR chloride channel (which fails to fold and traffic properly) by MG-132 resulted in a modest increase in its cell surface expression, as reflected by the post-Golgi glycoform (band C), in contrast to the results from the use of celastrol (Figures S11A and B) or high concentrations of MG-132 (Jensen et al., 1995).

PC and PR synergy in a Tay-Sachs cell line

2-Acetamido-2-deoxynojirimycin (ADNJ) functions as a PC in a number of Tay-Sachs patient-derived cell lines (Tropak et al., 2004). The compound heterozygous fibroblast cell line introduced above was exposed once to ADNJ without media changes (20 to 50 μM), affording a 2.5-fold (150 unit) increase in cellular HexA α-site activity (to ≈ 25% of WT HexA activity) after 192 h (Figure S10B). Co-administration of MG-132 (0.8 μM) and ADNJ (20 μM) yielded a 5-fold (400 unit) increase in αG269S Hex α-site activity (to ≈ 50% of WT HexA activity) 144 h after treatment (Figures 6F and S10C and D), which is greater than the 3.3-fold (230 unit) sum of the individual effects, again demonstrating synergy resulting from the combined use of a PR and a PC.

Discussion

We have demonstrated that improving the protein folding capacity of the cell results in improved mutant protein folding and function, to an extent capable of ameliorating loss-of-function diseases. While the PRs studied activate both the HSR and the UPR, it is the latter that appears to mediate the partial restoration of folding, trafficking and enzyme function, Figure 7, at least in the context of mutant lumenal lysosomal enzymes. Furthermore, it was recently reported that ER stress increases the expression of methylenetetrahydrofolate reductase through the IRE1 transducer (Leclerc and Rozen, 2008). While the importance of the UPR for PR function has been demonstrated, we cannot exclude the possibility that constitutive levels of cytosolic proteostasis components are important for enhancing secretory pathway proteostasis (Liu and Chang, 2008;Wiseman et al., 2007).

Using PRs to treat loss-of-function diseases is appealing because one molecule can be used for more than one disease, important considering that there are > 40 different LSDs (Beutler, 2006; Jeyakumar et al., 2002). While we showed that PRs can be used to restore partial enzyme function in two distinct LSD cell lines, the broader generality of PR utilization remains to be demonstrated. There is reason to be optimistic, as MG-132 also enhances ΔF508 CFTR folding and trafficking (Figure S11A) and has been previously reported to increase the surface

expression of mutant and wild type ATP-sensitive K^+ channels (Yan et al., 2005). Celastrol's narrow therapeutic window of 0.5 to ≈ 1 μM, resulting from cytotoxicity at higher concentrations, and the proteasome inhibition function of MG-132 would be concerns if these compounds were being pursued as drug candidates. Instead, they are used here for proof of principle and to motivate the discovery of less toxic and more specific equivalents.

We have also demonstrated that the combined use of a PR and an active site directed PC yields synergistic restoration of mutant enzyme function in Gaucher and Tay-Sachs disease patient derived fibroblasts. PRs activate the UPR (Figure 7), resulting in the coordinated transcription and translation of chaperones and folding enzymes that minimize mutant enzyme misfolding/aggregation and enhance folding efficiency. Thus, UPR activation increases the pool of folded mutant enzyme that the PC can bind to and stabilize. PC treatment "pulls" more mutant enzyme into the folded enzyme•PC state (Figure 7), increasing the concentration of the folded mutant enzyme that can engage the trafficking machinery for transport to the lysosome. The combination of a "push" towards the folded state by PRs and a "pull" toward the native state by PCs is substantially more effective than either would be alone. While our data are fully consistent with the suggested PR mechanism of action and the PR and PC synergy explanation, the effect of MG-132 and celastrol may be more complex than hypothesized.

In summary, we demonstrate that it is possible to treat two LSDs with a single PR, opening the possibility to treat several LSDs with a single PR. Moreover, we show that the combined use of a PR and a PC yields synergistic restoration of mutant enzyme function in Gaucher and Tay-Sachs fibroblasts owing to their distinct mechanisms of action discussed above. Optimization of the dosing schedule, chemistry and pharmacology of these and additional PRs, as well as enhancing the dosing strategies for the combined use of PCs and PRs offers the promise of yielding clinical candidates for LSDs and possibly other loss-of-function diseases.

Experimental Procedures

Enzyme activity assays

The intact cell GC activity assay using the MUG substrate (Sawkar et al., 2002) and the Hex α-site activity assay using the MUGS substrate (Tropak et al., 2004) have been previously described and are detailed in Supplemental Experimental Procedures. Trypan blue staining was utilized to measure cell viability. Each data point reported was evaluated at least in triplicate in each plate, and on three different days.

Western blot analysis

Cells were lysed with the complete lysis-M buffer containing complete protease inhibitor cocktail. Company specifications were followed for protein treatment with Endo H and PNGase F, respectively. Aliquots of cell lysates were separated in a 10% SDS-PAGE gel and western blot analysis was performed using appropriate antibodies. Bands in endo H treated samples were quantified by Java Image processing and analysis software from the NIH. For more detail, see Supplemental Experimental Procedures.

Immunofluorescence

Immunofluorescence was performed as described in (Sawkar et al., 2006b). Briefly, cells grown on glass cover slips were fixed with 3.7% paraformaldehyde in PBS for 15 min. The cover slips were washed with PBS, quenched with 15 mM glycine in PBS for 10 min, and the cells permeabilized with 0.2% saponin in PBS for 15 min. Cells were incubated for 1 hour with primary antibodies (1:100 for mouse monoclonal anti-GC 8E4 (kindly provided by Klaus-Peter Zimmer, Münster, Germany), and 1:10,000 for rabbit anti-LAMP2 (kindly provided by Michiko Fukuda, The Burnham Institute, La Jolla, CA)), washed with 5% goat serum in PBS,

and incubated for 1 h with secondary antibodies (Alexa Fluor 488 goat anti-mouse IgG and Alexa Fluor 546 goat anti-rabbit IgG from Molecular Probes). The cover slips were mounted and sealed. Images were collected using a Bio-Rad (Zeiss) Radiance 2100 Rainbow laser scanning confocal microscope attached to a Nikon TE2000-U microscope, and analyzed using NIH Image J software. The experiments were done three times and similar results were obtained.

Cell-based chymotrypsin-like proteasomal activity assay

Proteasome-Glo Cell-Based Assay kit (Promega, Madison, WI) was used to measure the chymotrypin-like proteasomal activity, as described in Supplemental Experimental Procedures.

Relative quantification of protein expression level changes by Multidimensional Protein Identification Technology (MudPIT)

Relative MudPIT protein quantification using spectra counting was used to analyze the concentration changes, as described in more detail in Supplemental Experimental Procedures and in the literature (Liu et al., 2004).

Quantitative RT-PCR

After reverse transcription, quantitative PCR reactions were performed using cDNA, QuantiTect SYBR Green PCR Kit (Qiagen) and corresponding primers (listed in Table S1) in the ABI PRISM 7900 system (Applied Biosystems). The ΔC_T value was used to describe the difference between the C_T of a target gene and the C_T of the housekeeping gene, GAPDH: $\Delta C_T = C_T$ (target gene) - C_T (GAPDH). The relative mRNA expression level of a target gene of drug-treated cells was normalized to that of untreated cells: Relative mRNA expression level = 2 exp [- (ΔC_T (treated cells) - ΔC_T (untreated cells))]. Each data point was evaluated in triplicate, and measured three times. For more detail, see Supplemental Experimental Procedures.

RT-PCR analysis of Xbp-1 splicing

After reverse transcription, PCR reactions were performed using cDNA, Taq DNA polymerase and appropriate primers listed in Table S1. PCR products were separated on a 2.5% agarose gel. Unspliced Xbp-1 yielded a 289 bp amplicon, and spliced Xbp-1 yielded a 263 bp amplicon. This experiment was performed three times and similar results were obtained. For more detail, see Supplemental Experimental Procedures.

siRNA transfection

L444P GC fibroblasts were seeded at approximately 2×10^5 cells per well in 6-well plates for protein or RNA analyses or 10^4 cells per well in 96-well plates for intact cell GC activity assay, respectively. Cells were allowed to reach ~80% confluency before transfection. The small interfering RNA (siRNA) duplexes were from Dharmacon: ON-TARGETplus SMARTpool ATF6 (L-009917-00) and PERK (L-004883-00), ON-TARGETplus Duplex HSF1 (J-012109-05), siGENOME SMARTpool IRE1α (M-004951-01), and siGENOME Non-Targeting siRNA (D-001210-01-05) as control. Cells were mock transfected or transfected with corresponding 50 nM siRNA using HiPerfect Transfection Reagent (Qiagen) according to the manufacturer's transfection protocol. Knockdown efficiency was evaluated after a 24 h siRNA pretreatment followed by a 24 h incubation with DMSO.

Statistical analysis

All data are presented as mean ± SEM or mean ± SD as stated.

Supplementary Material

Refer to Web version on PubMed Central for supplementary material.

Acknowledgments

We thank the reviewers for their insight, Professors Jonathan Weissman and Ernest Beutler for helpful discussions, Professor Evan Powers for the latter and for creating the three-dimensional plots used herein, Jonathan Zhu for significant help with the Figures. This work was supported by the NIH (DK75295), the Skaggs Institute of Chemical Biology, and the Lita Annenberg Hazen Foundation and is dedicated to Ernest Beutler on the occasion of his upcoming 80th birthday.

References

Albanese V, Yam AY-W, Baughman J, Parnot C, Frydman J. Systems analyses reveal two chaperone networks with distinct functions in eukaryotic cells. Cell 2006;124:75–88. [PubMed: 16413483]

Awasthi N, Wagner BJ. Upregulation of heat shock protein expression by proteasome inhibition: An antiapoptotic mechanism in the lens. Invest Ophthalmol Vis Sci 2005;46:2082–2091. [PubMed: 15914627]

Balch WE, Morimoto RI, Dillin A, Kelly JW. Adapting proteostasis for disease intervention. Science 2008;319:916–919. [PubMed: 18276881]

Beutler E. Lysosomal storage diseases: natural history and ethical and economic aspects. Mol Genet Metab 2006;88:208–215. [PubMed: 16515872]

Beutler E, Dale GL, Guinto E, Kuhl W. Enzyme replacement therapy in Gaucher's disease: Preliminary clinical trial of a new enzyme preparation. Proc Natl Acad Sci USA 1977;74:4620–4623. [PubMed: 200923]

Beutler E, Gelbart T, Scott CR. Hematologically important mutations: Gaucher disease. Blood Cells Mol Dis 2005;35:355–364. [PubMed: 16185900]

Bouvier M. When an inhibitor promotes activity. Chem Biol 2007;14:241–242. [PubMed: 17379138]

Boyce M, Bryant KF, Jousse C, Long K, Harding HP, Scheuner D, Kaufman RJ, Ma D, Coen DM, Ron D, et al. A selective inhibitor of eIF2alpha dephosphorylation protects cells from ER stress. Science 2005;307:935–939. [PubMed: 15705855]

Brady RO. Enzyme replacement for lysosomal diseases. Ann Rev Med 2006;57:283–296. [PubMed: 16409150]

Brodsky JL. The protective and destructive roles played by molecular chaperones during ERAD (endoplasmic-reticulum-associated degradation). Biochem J 2007;404:353–363. [PubMed: 17521290]

Brown CR, Hong-Brown LQ, Welch WJ. Correcting temperature-sensitive protein folding defects. J Clin Invest 1997;99:1432–1444. [PubMed: 9077553]

Bush KT, Goldberg AL, Nigam SK. Proteasome inhibition leads to a heat-shock response, induction of endoplasmic reticulum chaperones, and thermotolerance. J Biol Chem 1997;272:9086–9092. [PubMed: 9083035]

Chillaron J, Haas IG. Dissociation from BiP and retrotranslocation of unassembled immunoglobulin light chains are tightly coupled to proteasome activity. Mol Biol Cell 2000;11:217–226. [PubMed: 10637303]

Cohen FE, Kelly JW. Therapeutic approaches to protein-misfolding diseases. Nature 2003;426:905–909. [PubMed: 14685252]

Conzelmann E, Sandhoff K. Partial enzyme deficiencies: Residual activities and the development of neurological disorders. Dev Neurosci 1984;6:58–71. [PubMed: 6421563]

Deuerling E, Bukau B. Chaperone-assisted folding of newly synthesized proteins in the cytosol. Crit Rev Biochem Molec Biol 2004;39:261–277. [PubMed: 15763705]

Fan J-Q. Potential drug therapies for lysosomal storage disorders. Front Biotechnol Pharm 2001;2:275–291.

Fan J-Q, Ishii S, Asano N, Suzuki Y. Accelerated transport and maturation of lysosomal α-galactosidase A in Fabry lymphoblasts by an enzyme inhibitor. Nat Med 1999;5:112–115. [PubMed: 9883849]

Futerman AH, van Meer G. The cell biology of lysosomal storage disorders. Nat Rev Mol Cell Biol 2004;5:554–565. [PubMed: 15232573]

Horwich AL, Fenton WA, Farr GW. Chaperonins. Encyclopedia Biol Chem 2004;1:393–398.

Imai J, Yashiroda H, Maruya M, Yahara I, Tanaka K. Proteasomes and molecular chaperones. Cellular machinery responsible for folding and destruction of unfolded proteins. Cell Cycle 2003;2:585–589. [PubMed: 14512774]

Jensen TJ, Loo MA, Pind S, Williams DB, Goldberg AL, Riordan JR. Multiple proteolytic systems, including the proteasome, contribute to CFTR processing. Cell 1995;83:129–135. [PubMed: 7553864]

Jeyakumar M, Butters TD, Dwek RA, Platt FM. Glycosphingolipid lysosomal storage diseases: therapy and pathogenesis. Neuropathol Appl Neurobiol 2002;28:343–357. [PubMed: 12366816]

Kaufman RJ. Orchestrating the unfolded protein response in health and disease. J Clin Invest 2002;110:1389–1398. [PubMed: 12438434]

Leclerc D, Rozen R. Endoplasmic reticulum stress increases the expression of methylenetetrahydrofolate reductase through the IRE1 transducer. J Biol Chem 2008;283:3151–3160. [PubMed: 18065414]

Liao L, Pilotte J, Xu T, Wong CCL, Edelman GM, Vanderklish P, Yates JR. BDNF induces widespread changes in synaptic protein content and up-regulates components of the translation machinery: An analysis using high-throughput proteomics. J Proteome Res 2007;6:1059–1071. [PubMed: 17330943]

Liao W, Li X, Mancini M, Chan L. Proteasome inhibition induces differential heat shock protein response but not unfolded protein response in HepG2 cells. J Cell Biochem 2006;99:1085–1095. [PubMed: 16767695]

Lindquist S. The heat-shock response. Ann Rev Biochem 1986;55:1151–1191. [PubMed: 2427013]

Liu HB, Sadygov RG, Yates JR. A model for random sampling and estimation of relative protein abundance in shotgun proteomics. Anal Chem 2004;76:4193–4201. [PubMed: 15253663]

Liu Y, Chang A. Heat shock response relieves ER stress. EMBO J 2008;27:1049–1059. [PubMed: 18323774]

Maegawa GHB, Tropak M, Buttner J, Stockley T, Kok F, Clarke JTR, Mahuran DJ. Pyrimethamine as a potential pharmacological chaperone for late-onset forms of GM2 gangliosidosis. J Biol Chem 2007;282:9150–9161. [PubMed: 17237499]

Morimoto RI. Regulation of the heat shock transcriptional response: cross talk between a family of heat shock factors, molecular chaperones, and negative regulators. Genes Dev 1998;12:3788–3796. [PubMed: 9869631]

Moyer BD, Balch WE. A new frontier in pharmacology: The endoplasmic reticulum as a regulated export pathway in health and disease. Emerg Ther Targets 2001;5:165–176.

Mu TW, Fowler DM, Kelly JW. Partial restoration of mutant enzyme homeostasis in three distinct lysosomal storage disease cell lines by altering calcium homeostasis. PLoS Biol 2008;6:e26. [PubMed: 18254660]

Rikova K, Guo A, Zeng Q, Possemato A, Yu J, Haack H, Nardone J, Lee K, Reeves C, Li Y, et al. Global survey of phosphotyrosine signaling identifies oncogenic kinases in lung cancer. Cell 2007;131:1190–1203. [PubMed: 18083107]

Ron D, Walter P. Signal integration in the endoplasmic reticulum unfolded protein response. Nat Rev Mol Cell Biol 2007;8:519–529. [PubMed: 17565364]

Ron I, Horowitz M. ER retention and degradation as the molecular basis underlying Gaucher disease heterogeneity. Hum Mol Genet 2005;14:2387–2398. [PubMed: 16000318]

Sawkar AR, Adamski-Werner SL, Cheng WC, Wong CH, Beutler E, Zimmer KP, Kelly JW. Gaucher disease-associated glucocerebrosidases show mutation-dependent chemical chaperoning profiles. Chem Biol 2005;12:1235–1244. [PubMed: 16298303]

Sawkar AR, Cheng WC, Beutler E, Wong CH, Balch WE, Kelly JW. Chemical chaperones increase the cellular activity of N370S beta-glucosidase: a therapeutic strategy for Gaucher disease. Proc Natl Acad Sci U S A 2002;99:15428–15433. [PubMed: 12434014]

Sawkar AR, D'Haeze W, Kelly JW. Therapeutic strategies to ameliorate lysosomal storage disorders--a focus on Gaucher disease. Cell Mol Life Sci 2006a;63:1179–1192. [PubMed: 16568247]

Sawkar AR, Schmitz M, Zimmer KP, Reczek D, Edmunds T, Balch WE, Kelly JW. Chemical chaperones and permissive temperatures alter the cellular localization of Gaucher disease associated glucocerebrosidase variants. ACS Chem Biol 2006b;1:235–251. [PubMed: 17163678]

Schmitz M, Alfalah M, Aerts JMFG, Naim HY, Zimmer KP. Impaired trafficking of mutants of lysosomal glucocerebrosidase in Gaucher's disease. Int J Biochem Cell Biol 2005;37:2310–2320. [PubMed: 15982918]

Schroeder M, Kaufman RJ. The mammalian unfolded protein response. Ann Rev Biochem 2005;74:739–789. [PubMed: 15952902]

Schueler UH, Kolter T, Kaneski CR, Zirzow GC, Sandhoff K, Brady RO. Correlation between enzyme activity and substrate storage in a cell culture model system for Gaucher disease. J Inherit Metab Dis 2004;27:649–658. [PubMed: 15669681]

Tropak MB, Reid SP, Guiral M, Withers SG, Mahuran D. Pharmacological enhancement of beta-hexosaminidase activity in fibroblasts from adult Tay-Sachs and Sandhoff Patients. J Biol Chem 2004;279:13478–13487. [PubMed: 14724290]

Ulloa-Aguirre A, Janovick JA, Brothers SP, Conn PM. Pharmacologic rescue of conformationally-defective proteins: implications for the treatment of human disease. Traffic 2004;5:821–837. [PubMed: 15479448]

Wang X, Venable J, LaPointe P, Hutt DM, Koulov AV, Coppinger J, Gurkan C, Kellner W, Matteson J, Plutner H, et al. Hsp90 cochaperone Aha1 downregulation rescues misfolding of CFTR in cystic fibrosis. Cell 2006;127:803–815. [PubMed: 17110338]

Westerheide SD, Bosman JD, Mbadugha BN, Kawahara TL, Matsumoto G, Kim S, Gu W, Devlin JP, Silverman RB, Morimoto RI. Celastrols as inducers of the heat shock response and cytoprotection. J Biol Chem 2004;279:56053–56060. [PubMed: 15509580]

Westerheide SD, Morimoto RI. Heat shock response modulators as therapeutic tools for diseases of protein conformation. J Biol Chem 2005;280:33097–33100. [PubMed: 16076838]

Wiseman RL, Powers ET, Buxbaum JN, Kelly JW, Balch WE. An adaptable standard for protein export from the endoplasmic reticulum. Cell 2007;131:809–821. [PubMed: 18022373]

Yam GHF, Bosshard N, Zuber C, Steinmann B, Roth J. Pharmacological chaperone corrects lysosomal storage in Fabry disease caused by trafficking-incompetent variants. Am J Physiol-Cell Physiol 2006;290:C1076–C1082. [PubMed: 16531566]

Yan F-F, Lin C-W, Cartier EA, Shyng S-L. Role of ubiquitin-proteasome degradation pathway in biogenesis efficiency of β-cell ATP-sensitive potassium channels. Am J Physiol 2005;289:C1351–C1359.

Yang H, Chen D, Cui QC, Yuan X, Dou QP. Celastrol, a triterpene extracted from the Chinese "Thunder of God Vine," is a potent proteasome inhibitor and suppresses human prostate cancer growth in nude mice. Cancer Res 2006;66:4758–4765. [PubMed: 16651429]

Young JC, Agashe VR, Siegers K, Hartl FU. Pathways of chaperone-mediated protein folding in the cytosol. Nat Rev Mol Cell Biol 2004;5:781–791. [PubMed: 15459659]

Yu Z, Sawkar AR, Whalen LJ, Wong C-H, Kelly JW. Isofagomine- and 2,5-anhydro-2,5-imino-D-glucitol-based glucocerebrosidase pharmacological chaperones for Gaucher disease intervention. J Med Chem 2007;50:94–100. [PubMed: 17201413]

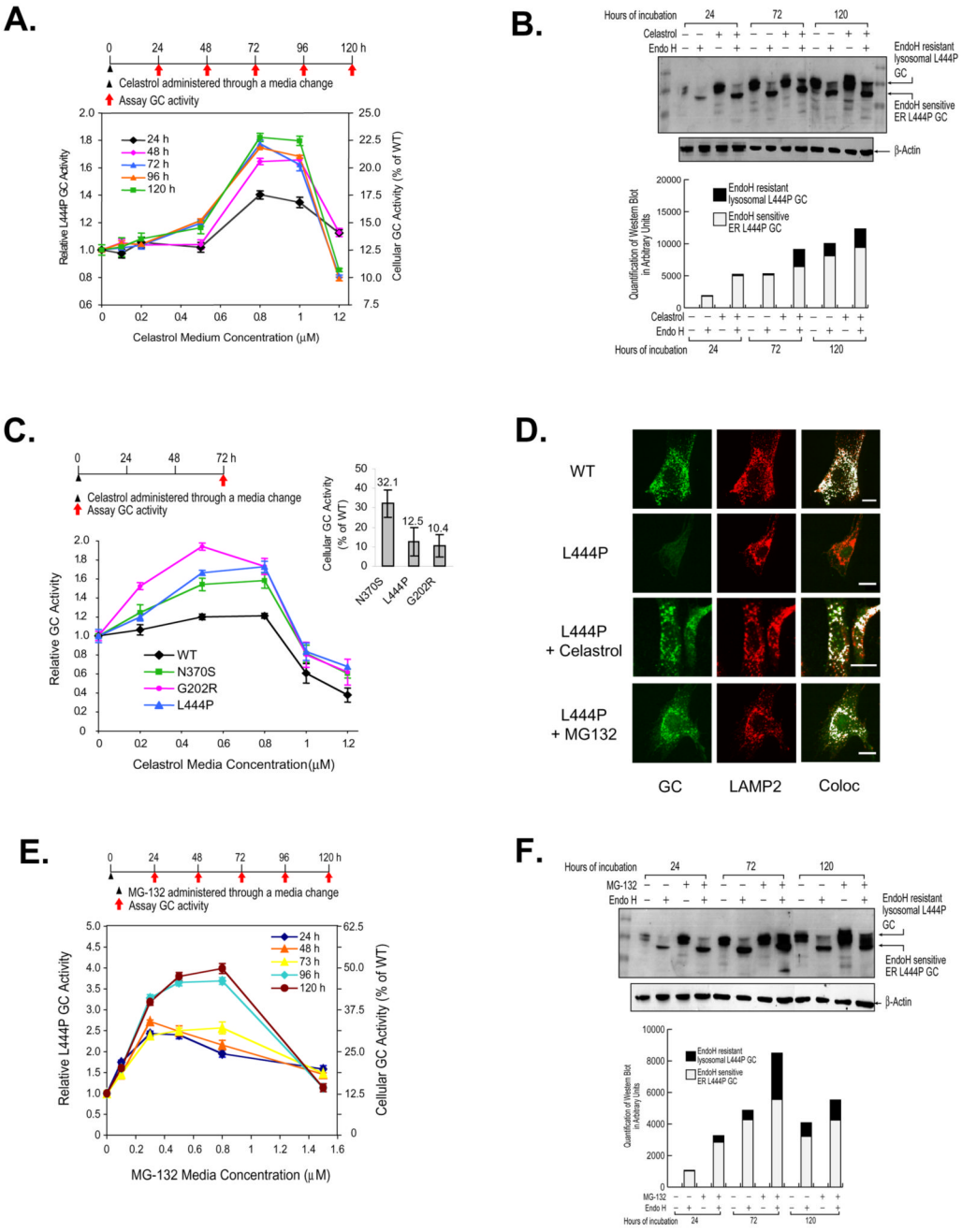

Figure 1.

Celastrol or MG-132 treatment enhances folding, trafficking and activity of glucocerebrosidases (GCs) variants. Relative lysosomal GC activity of L444P GC fibroblasts upon celastrol (**A**) or MG-132 (**E**) treatment. Reported activities were normalized to the activity of untreated cells of the same type (left y axis) and expressed as the percentage of WT GC activity (right y axis). Western blot analysis of L444P GC trafficking within fibroblasts after 24, 72, and 120 h exposure to 0.8 μM celastrol (**B**) or 0.8 μM MG-132 (**F**). The white portion of the bars represents quantification (Java Image processing and analysis software from the NIH) of the lower, endo H sensitive bands and the black portion of the bars represents the higher MW, endo H resistant post-Golgi glycoform. Relative lysosomal activity of WT GC

and Gaucher disease-associated N370S, G202R, and L444P GC variants (**C**) in patient-derived fibroblasts. The inset displays GC variant enzyme activity expressed as a percentage of WT GC activity, as reported previously (Sawkar et al., 2005). The data in (**A**), (**C**) and (**E**) were reported as mean ± SEM. Immunofluorescence microscopy of GC (**D**) in L444P fibroblasts and WT cells (positive control). L444P GC cells were untreated (second row) or incubated with 0.8 μM celastrol (third row) or 0.25 μM MG-132 (bottom row) for 3 days. GC was detected using the mouse anti-GC antibody 8E4 (column 1); rabbit anti-LAMP2 antibody was used as a lysosomal marker (column 2). Colocalization of GC (green) and LAMP2 (red) was artificially colored white (column 3). Bar equals 20 μM.

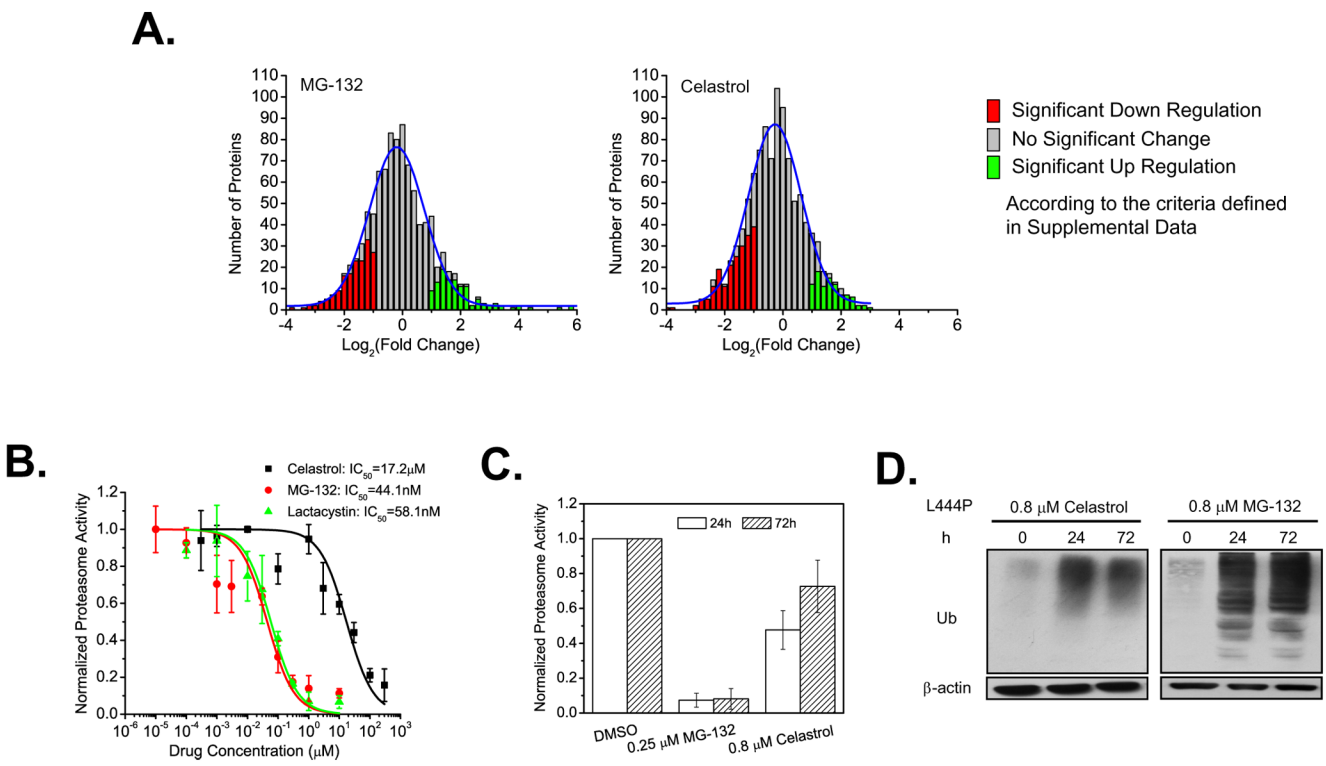

Figure 2.

Influence of celastrol and MG-132 on proteostasis. Changes in the L444P GC fibroblast proteome (**A**) after MG-132 (0.8 μM) or celastrol (0.8 μM) treatment for 72 h. The number of proteins is plotted against fold change using a normalized spectra count ratio of drug treated samples versus untreated samples in cases where a given protein is detected in both untreated and treated samples. Dose-response curves (**B**) of the inhibition of the chymotrypsin-like activity of the proteasome by celastrol, MG-132, or lactacystin in L444P GC cells. Chymotrypsin-like activity of the proteasome (**C**) in L444P GC cells incubated with celastrol (0.8 μM) or MG-132 (0.25 μM) for 24 h and 72 h. The data were reported as mean ± SD in (**B**) or as mean ± SEM in (**C**). Western blot analysis of ubiquitinated proteome (**D**) in L444P GC fibroblasts after 0.8 μM celastrol or MG-132 treatment for 24 h and 72 h.

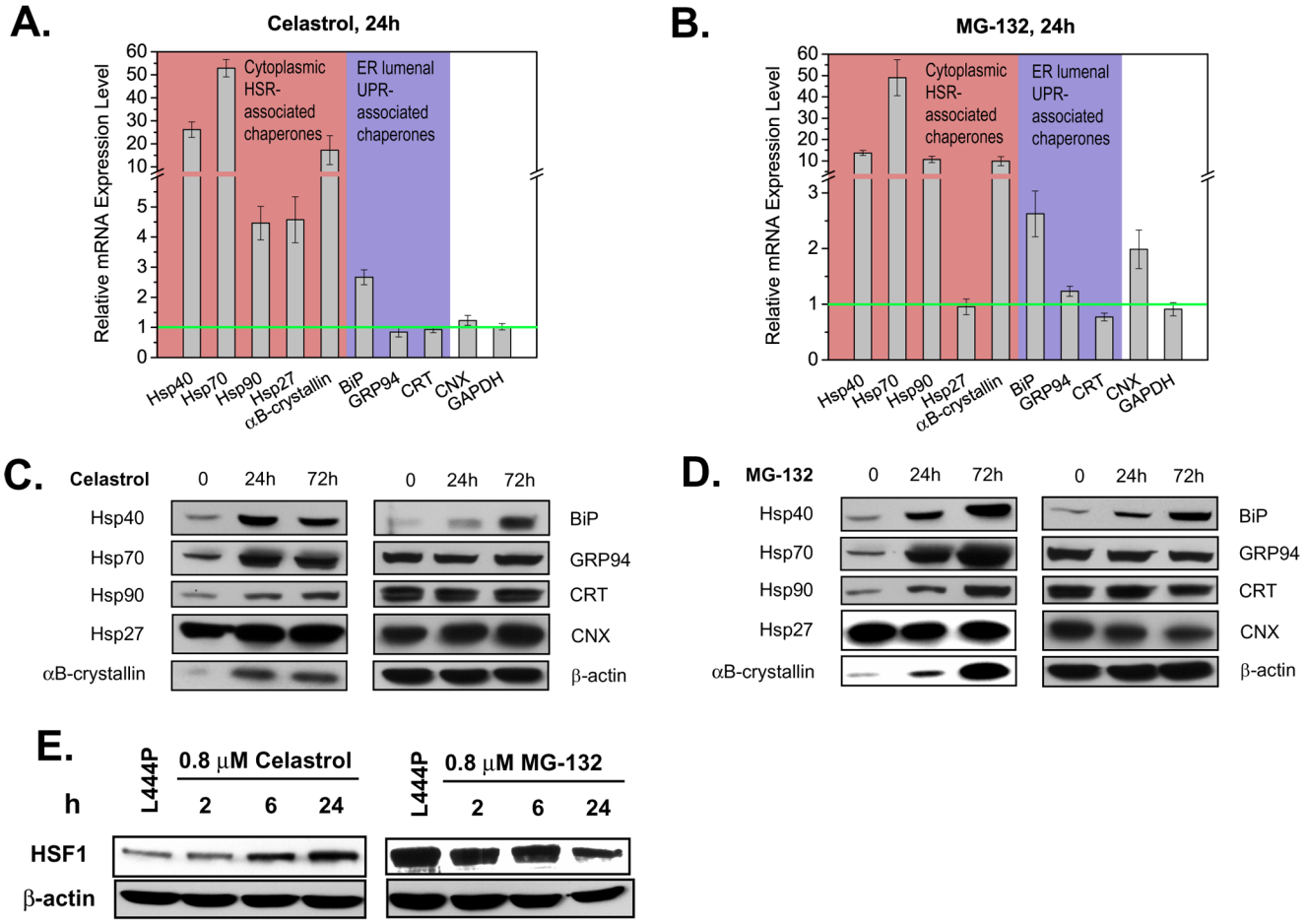

Figure 3.

Both MG-132 and celastrol activate the HSR in L444P GC fibroblasts. Relative chaperone mRNA expression probed by quantitative RT-PCR in cells treated with 0.8 μM celastrol (**A**) or 0.8 μM MG-132 (**B**) for 24 h. Relative mRNA expression level for treated L444P GC cells normalized to that of untreated cells after correction for the expression level of GAPDH, a housekeeping control. The data in (**A**) and (**B**) were reported as mean ± SEM. Western blot analyses in L444P GC fibroblasts treated with 0.8 μM celastrol (**C**) or 0.8 μM MG-132 (**D**) for 24 h or 72 h. HSF1 protein expression levels (**E**) in L444P GC cells treated with 0.8 μM celastrol and 0.8 μM MG-132.

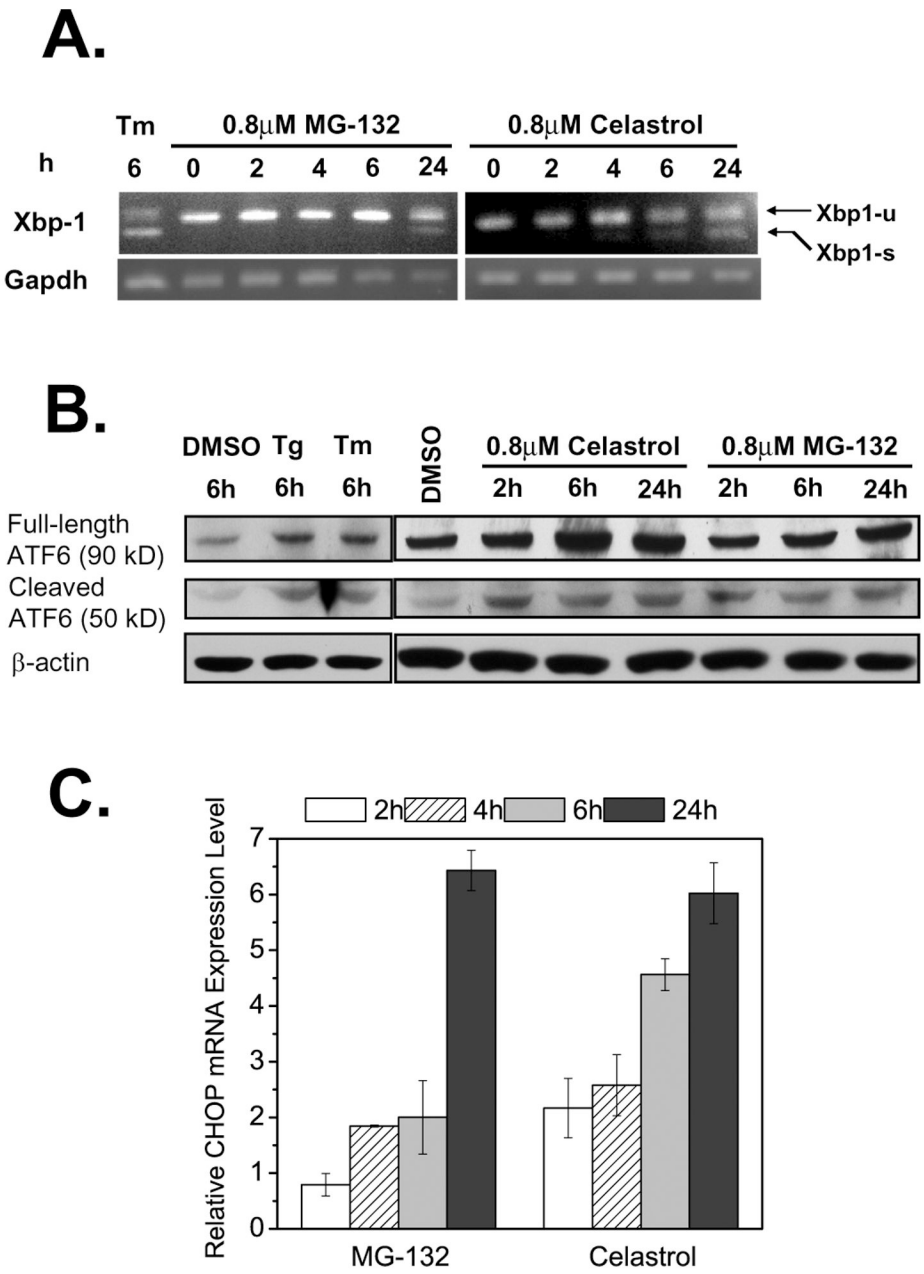

Figure 4.

Activation of the UPR by MG-132 and celastrol. Detection of spliced Xbp-1 mRNA by RT-PCR (**A**) in L444P GC fibroblasts treated with 0.8 μM MG-132 or 0.8 μM celastrol (tunicamycin (Tm) is a positive control, GAPDH, a housekeeping control). Xbp1-u represents unspliced Xbp-1, and Xbp1-s represents spliced Xbp-1. Cleavage of ATF6 proteins revealed by Western blotting (**B**) in celastrol or MG-132 treated L444P GC cells (thapsigargain (Tg) and Tm served as positive controls). Relative mRNA expression levels of CHOP (**C**) probed by quantitative RT-PCR in L444P GC fibroblasts treated with 0.8 μM celastrol or MG-132. Relative mRNA expression level for treated L444P GC cells was normalized to that of untreated

cells after correction for the expression level of GAPDH. The data in (**C**) were reported as mean ± SEM.

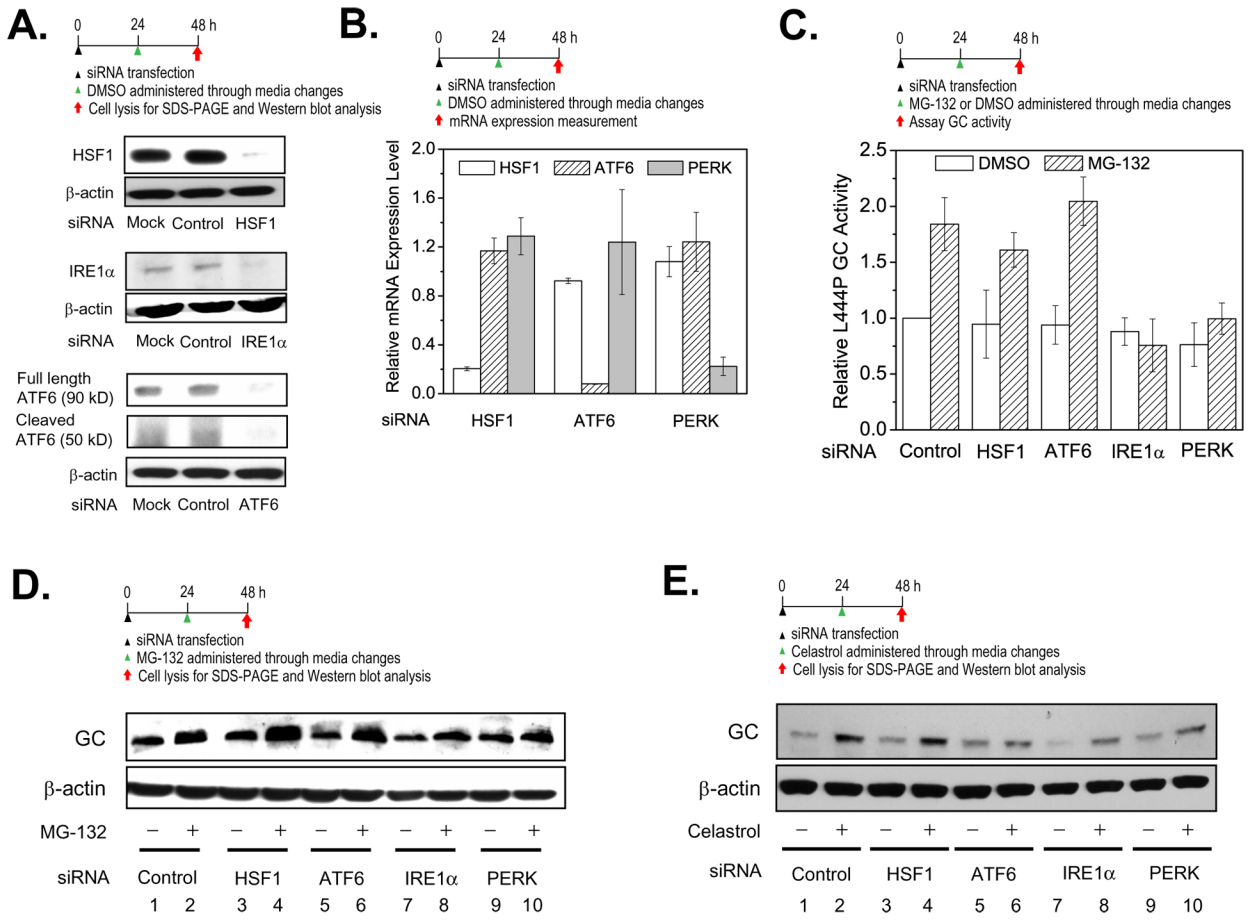

Figure 5.

The UPR, but not the HSR, is important for PR function. Knockdown of HSF1, IRE1α, and ATF6 (**A**) by siRNA lasts at least 48 h, according to Western blot analysis. Relative mRNA expression levels of HSF1, ATF6 and PERK were probed by quantitative RT-PCR to verify knockdown of HSF1, ATF6 and PERK (**B**) in L444P GC fibroblasts after specific siRNA treatment—mRNA expression levels normalized to that of non-targeting siRNA treated cells after correction for GAPDH levels. siRNA knockdown of IRE1α or PERK (**C**) blocks the ability of MG-132 (0.25 μM in DMSO) to increase L444P GC activity, activities normalized to L444P GC cells treated with both non-targeting siRNA (control) and DMSO vehicle. The data in (**B**) and (**C**) were reported as mean ± SD. Western blot analysis of L444P GC in fibroblasts treated with non-targeting siRNA (control) plus DMSO (vehicle) or HSF1, IRE1α, ATF6 and PERK siRNAs without (just DMSO vehicle) or with 0.25 μM MG-132 (**D**) or 0.8 μM celastrol (**E**) in DMSO.

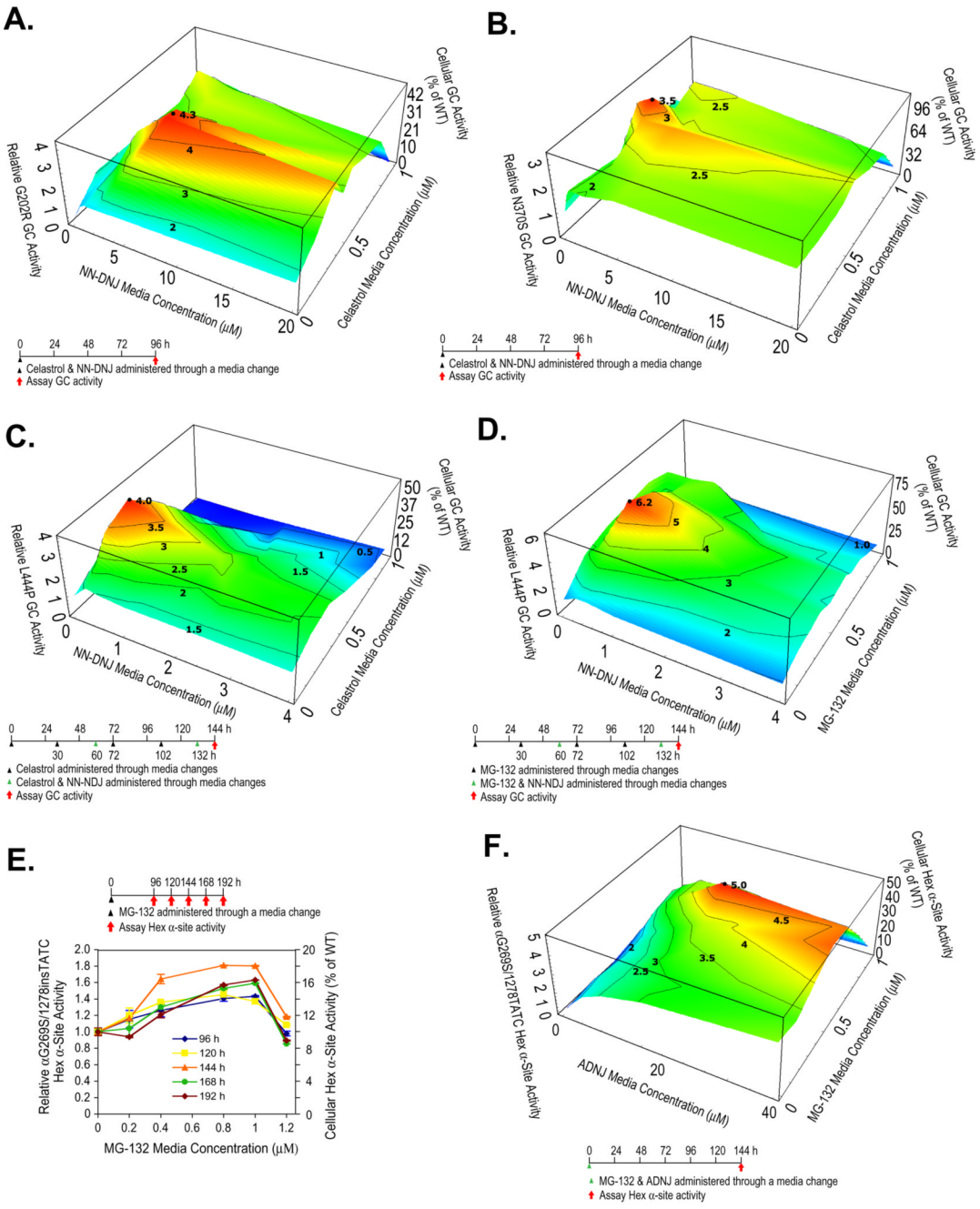

Figure 6.

PCs and PRs exhibit synergy in Gaucher and Tay-Sachs fibroblasts. Enzyme activities within patient-derived fibroblasts treated with a PC and a PR. In all the 3D plots (**A–D**, and **F**), PR and PC media concentrations are shown on the x and y-axes, and the mutant enzyme activities on the z-axis with the dosing schematic depicted at the bottom. Reported activities were normalized to the activity of untreated cells of the same type (left z axis) and expressed as the percentage of WT enzyme activity (right z axis). αG269S/1278insTATC HexA fibroblasts were exposed to MG-132 (**E**) and the Hex α-site activities were measured as a function of time. The data in (**E**) were reported as mean ± SEM.

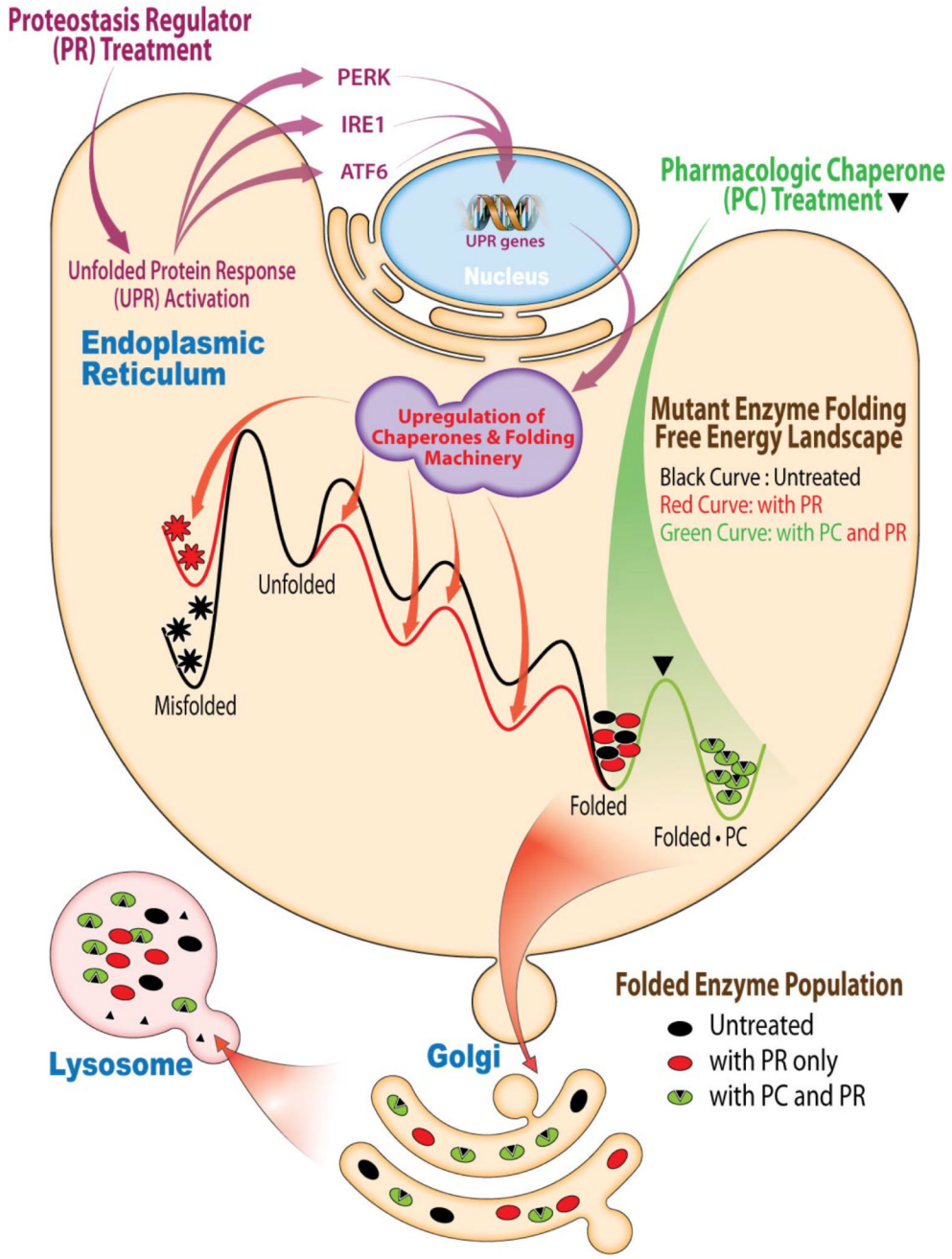

Figure 7.

PRs and PCs synergize to restore mutant enzyme homeostasis. PRs activate the UPR, resulting in the coordinated transcription and translation of chaperones and folding enzymes that resculpt the folding free energy diagram of the mutant enzyme in the ER, enhancing its folding and minimizing misfolding, which increases the population of the mutant enzyme in the folded state. PCs bind to the folded state of the mutant enzyme, further stabilizing it, which further increases its population. Together these mechanisms of action are more effective at increasing the concentration of the folded mutant enzyme and folded mutant enzyme•PC complex, both of which can engage the trafficking machinery, increasing mutant enzyme lysosomal concentration and activity.